




Graded-azimuthal-index fiber as a control element for radial-index and orbital-angular-momentum modes of Laguerre-Gaussian beams

S. Srinivasu ^{1,*} and H. Wanare ^{1,2,†}

¹Center for Lasers and Photonics, Indian Institute of Technology Kanpur, Kanpur, Uttar Pradesh 208016, India

²Department of Physics, Indian Institute of Technology Kanpur, Kanpur, Uttar Pradesh 208016, India

 (Received 22 July 2022; revised 22 December 2022; accepted 23 December 2022; published 23 January 2023)

We propose an azimuthally varying graded-index fiber that can efficiently create and control a definite set of radial-index and orbital-angular-momentum (OAM) modes of Laguerre-Gaussian beams and their superpositions. A rigorous coupled-wave analysis formalism is developed, which provides a ready analysis for the azimuthal-refractive-index variation in the Laguerre-Gaussian basis. In particular, we present effective control in the generation and coupling of the various OAM modes, including radial-index modes of the Laguerre-Gaussian beam within the fiber, wherein the propagation length of the fiber and the wavelength act as the control parameters. We further present the possibility of switching every alternate channel in a wavelength division multiplexing protocol to a higher-order spatial mode within the optical fiber to substantially reduce interchannel crosstalk. The graded azimuthal index fiber can be utilized in high-speed fiber-optic communications as a versatile control element for OAM modes and the radial-index mode of the Laguerre-Gaussian beam transformation.

DOI: [10.1103/PhysRevA.107.013517](https://doi.org/10.1103/PhysRevA.107.013517)

I. INTRODUCTION

In recent times, the orbital-angular-momentum (OAM) content of the light field has been sought as a key element in a plethora of applications ranging from microscopy and material processing to quantum information processing [1–5]. Efficient generation, manipulation, and detection of the OAM content are central to this degree of freedom being adapted in myriad applications. As of now, the development of OAM-centric tools (both theoretical and experimental) is far from optimal. In this paper we propose an efficient regime of generation and effective manipulation of the OAM and its superposition states, including the radial-index mode of the Laguerre-Gaussian (LG) beam. One critical limitation is that most of the azimuthal phase-varying tools avoid accounting for the radial-index modes of the LG beam. The spatial light modulator (SLM) considers only the generation of OAM modes without offering any further control over the propagation-related coupling between the modes. Therefore, we present the analysis, incorporating all the degrees of freedom (DOF), namely, the azimuthal (l) index and radial (p) index of the LG beam, and their interaction along the propagation direction.

Furthermore, having an equivalent fiber-based optical element that can be integrated with the conventional fiber-optic communication channel and support optical processing without bulk optical elements is an extremely attractive proposition. The fiber-equivalent optical elements offer a compact, potentially reliable, and efficient optical control element [5–7]. Fiber-based optical systems such as fiber lasers,

multiresonant fiber-grating-based sensors [8], and fiber-based systems with tunable spatial light generation [7], long periodic fiber gratings that generate OAM beams, are all critical optical control systems in this domain [9,10]. All these fibers involve refractive-index perturbations along the propagation direction z . Besides that, radially refractive-index-varying fiber designs have been investigated, such as the typical graded-index (GRIN) fibers, which support propagation of OAM modes over long distances [11], and GRIN elements in a cascading manner are used to generate vector vortex beams [12]. At the same time, specialty fiber designs for OAM mode propagation are being pursued, such as the ring-core vortex fiber, which supports the propagation-invariant LG OAM mode and offers less crosstalk among the supported OAM modes by increasing effective refractive-index separation [13]. All the above fiber designs are studied as propagation channels and offer little control over modal manipulation.

Along this line of thought, our proposed graded azimuthal index (GRAIN), in conjunction with the radial parabolic variation, offers a paradigm of spatial mode control. There have been a few fiber designs that contain azimuthal-refractive-index variation, for instance, multicore fibers [14,15], where cores are arranged in an azimuthal direction, and twisted photonic crystal fibers [16], where photonic band gaps are realized in the transverse dimension to guide the light along the fiber for a specific range of wavelengths. Furthermore, azimuthal coupling is proposed in a radial step change at the core and cladding boundary wherein the discontinuity increases or decreases along the azimuthal axis without any radial variation of the refractive index, which supports propagation of the specifically handed OAM modes [17,18]. Again, all the above-mentioned azimuthal coupling designs have been investigated as propagation channels and the guiding principle has been to preserve the supermode structure along the

*ssrinu@iitk.ac.in

†hwanare@iitk.ac.in

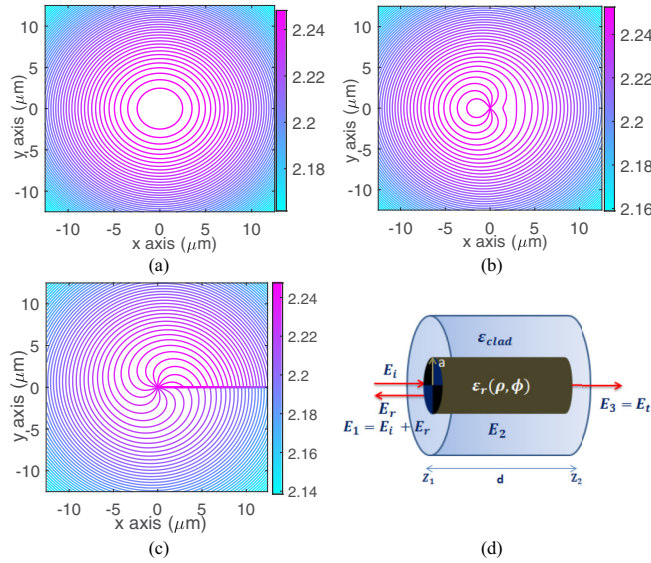


FIG. 1. (a) Typical GRIN fiber relative permittivity contour lines in the x - y plane. The proposed GRAIN fiber contour lines are for (b) $\bar{\epsilon}(\phi) = h \cos(\phi)$ and (c) $\bar{\epsilon}(\phi) = h\phi$ including the radial parabolic refractive index. (d) Notation involving the GRAIN fiber element

propagation direction. Thus, the significant difference in our work is that we exploit the azimuthal coupling as a control knob for manipulating spatial OAM modes, including the radial-index modes of the LG beam, which have been neglected so far [19].

We also construct the relevant theoretical framework, whereas all previously mentioned fiber designs are based on coupled-mode theory with modal couplings [10,14,20,21], for example, the tilted fiber Bragg grating considers the coupling of cladding modes [22]. However, ours is a generalized azimuthal coupling of spatial modes and a rigorous coupled-wave framework in the LG basis, which brings out the control aspects of spatial LG modes. In addition, the LG basis allows a seamless description of modes from fiber to free space. Like the spectral resonance within a wavelength range in fiber Bragg gratings [22], we provide the spatial mode resonance and switching for wavelength channels. Since our theoretical tool accounts for general azimuthal-refractive-index variation in the GRIN, we provide the results for the azimuthally increasing function of the refractive index [as shown in Fig. 1(c)], which is sensitive to the handedness of the OAM mode in both phase and intensity. The azimuthal cosinusoidal variation of the refractive index [as shown in Fig. 1(b)] is insensitive to the handedness of the OAM mode of its intensity, but the phase shift acquired by each handedness of the OAM mode differs. Any other arbitrary azimuthal dependence can easily be incorporated within this mathematical treatment. As a result, our work provides a comprehensive and rigorous model for azimuthal-refractive-index-coupled fibers, as well as mode selection based on propagation length. Most importantly, wavelength switching in the azimuthal DOF (l index) and radial DOF (p index) of the LG beam would help in high-speed mode-division-multiplexing-based optical communications.

In the theoretical framework, we provide correction terms to the conventional fiber dispersion arising due to the

azimuthal coupling. However, we ensure that the azimuthal refractive index is weaker than the radial-refractive-index variation such that it does not affect the radial cutoff criteria for the GRIN fiber modes. Because of the azimuthal coupling, the LG modes are coupled across the radial index (p index) and azimuthal DOF (l index). We solve the coupled differential equations rigorously in the eigenvalue problem framework along the lines of rigorous coupled-wave analysis (RCWA) in the literature [23]. Note that our RCWA treatment is in the LG beam basis, unlike the conventional plane-wave basis.

Furthermore, we address the crosstalk problem in the conventional wavelength division multiplexing (WDM) protocol. Traditionally, all the channels operate at the fundamental mode of the single-mode fiber. Therefore, a significant field overlap across adjacent channels limits the information transfer rate due to crosstalk [24]. One efficient way of addressing this lacuna would be to shift the adjacent modes to a higher-order spatial mode, thus drastically bringing down the crosstalk. We demonstrate the switching of alternate wavelength channels into a higher-order fiber mode using the GRAIN fiber element, thus minimizing the adjacent channel crosstalk and simultaneously scaling up high-speed optical communications. Moreover, spatial mode generation has recently been realized at the source as in a laser using SLM, q plates, and J plates [25]; however, fiber-based spatial light lasers have yet to be demonstrated. Therefore, our work offers such a possibility by including azimuthal-refractive-index variation in a typical fiber laser to generate spatially structured light at the source.

The organization of the paper is as follows. In Sec. I we review the importance of fiber elements and various specialty fiber structures related to the graded refractive index. In Sec. II we develop the theory of azimuthal-refractive-index coupling in the GRIN fiber element in the LG basis. In Sec. III we discuss the results for two particular cases of the GRAIN, such as cosinusoidal and linear azimuthal-refractive-index variation (as shown in Fig. 1). The wavelength-switching ability of such azimuthal-refractive-index variation is studied and discussed explicitly. Section IV concludes with the highlights of the paper.

II. THEORY OF GRADED-AZIMUTHAL-INDEX FIBER

We present a detailed theoretical model for the azimuthal variation of the refractive index in the GRIN fiber that allows us to work in the LG basis, wherein the OAM content and radial-index modes of the LG beam are indexed through the integers l and p , respectively. We consider a GRAIN fiber whose refractive-index variation is along both the radial ρ and azimuthal ϕ directions, and the relative permittivity of such a medium can be written in the direct product form as

$$\epsilon_r(\rho, \phi) = \epsilon(\rho)\epsilon(\phi), \quad (1)$$

where

$$\epsilon(\rho) = \epsilon_2 \left[1 - 2\Delta \left(\frac{\rho}{a} \right)^2 \right] \quad (2)$$

and

$$\epsilon(\phi) = 1 + \bar{\epsilon}(\phi) = 1 + \sum_{q \neq 0} \bar{\epsilon}_q e^{iqm_0\phi}, \quad (3)$$

where $\varepsilon_2 = n_{\text{core}}^2$ is the average relative permittivity of the core medium, Δ is defined as $(n_{\text{core}} - n_{\text{clad}})/n_{\text{core}}$, a is radius of the core, m_0 is the angular period of the medium [$m_0 = 2\pi/\phi_0$, $m_0 \in \mathbb{Z}^+$ (positive integer)], and $q \in \mathbb{Z}$ (integer) and $\bar{\varepsilon}_q$ are the spatial Fourier amplitudes.

Inside the dielectric GRAIN medium,

$$\vec{\nabla} \cdot \vec{D} = 0, \quad (4)$$

where $\vec{D} = \varepsilon_0 \varepsilon_r(\rho, \phi) \vec{E}$ and the corresponding wave equation within the medium is

$$\vec{\nabla}(\vec{\nabla} \cdot \vec{E}) - \nabla^2 \vec{E} = k_0^2 \varepsilon_r(\rho, \phi) \vec{E}, \quad (5)$$

where $k_0^2 = \omega^2/c^2$. It is well known that the field associated with the beamlike solution within the GRAIN medium does not satisfy the condition $\vec{\nabla} \cdot \vec{E} = 0$. There exist correction terms to the beamlike solutions. In a weakly modulating GRAIN medium, the higher-order corrections associated with the divergence term in Eq. (5) become negligible compared to the leading zeroth-order term, akin to the free-space situation. In effect, we solve the wave equation perturbatively by considering the electromagnetic wave to be linearly polarized along \hat{x} ; the spatial dependence of the electric field is given by

$$E_x(\rho, \phi, z) = \sum_n g^n E_x^{(n)}(\rho, \phi, z) \quad (6)$$

by substituting Eq. (6) in Eq. (5), and retaining the lowest order (g^0) term, we obtain

$$\nabla^2 E_x^{(0)} + k_0^2 \varepsilon_r(\rho, \phi) E_x^{(0)} = 0. \quad (7)$$

The solution of the wave equation (7) is expressed in the LG basis as

$$E_x = E_x^{(0)}(\rho, \phi, z) = \sum_{l,p} S_{l,p}(z) \text{LG}_l^p(\rho) e^{il\phi} e^{ik_2(z-z_1)}, \quad (8)$$

where $S_{l,p}(z)$ are the amplitude weight factors, with

$$\text{LG}_l^p(\rho) = \frac{C_{l,p}}{\sqrt{2}\rho_0} \left(\frac{\rho}{\rho_0}\right)^{|l|} e^{-\rho^2/2\rho_0^2} L_p^{|l|} \left(\frac{\rho^2}{\rho_0^2}\right),$$

where l is the OAM mode index with $l \in \mathbb{Z}$ (integer), p is the radial-index mode of the LG beam, which signifies $p+1$ and p minima along the radial direction for $l > 0$ and $l = 0$, respectively, L_p^l is the associated Laguerre polynomial,

$$C_{l,p} = \sqrt{2p!/\pi(p+|l|)!}$$

is the normalization constant, where ρ_0 is defined as a/\sqrt{V} , V is the normalized frequency (or V parameter), given as $V = k_0 a \sqrt{(n_{\text{core}}^2 - n_{\text{clad}}^2)}$ with $k_2^2 = k_0^2 \varepsilon_2$, and z_1 is the starting position of the GRAIN fiber medium [namely, the input interface, as shown in Fig. 1(d)].

We obtain the following coupled differential equation (15) for $S_{l,p}(z)$ by substituting Eqs. (1)–(3) and (8) in (7). We also identify the governing differential equation for the LG beam in the GRIN medium,

$$\left(\frac{\partial^2}{\partial \rho^2} + \frac{1}{\rho} \frac{\partial}{\partial \rho} + \left\{k_2^2 \left[1 - 2\Delta \left(\frac{\rho}{a}\right)^2\right] - \frac{l^2}{\rho^2}\right\}\right) \text{LG}_l^p = \beta_{l,p}^2 \text{LG}_l^p, \quad (9)$$

by considering Eq. (9) as the differential operator form $\hat{\mathbf{H}}_0 \text{LG}_l^p = \beta_{l,p}^2 \text{LG}_l^p$, where $\beta_{l,p}^2$ is given as

$$\beta_{l,p}^2 = k_2^2 \left(1 - (|l| + 2p + 1) \frac{4\Delta}{V}\right). \quad (10)$$

However, due to the product term $2\Delta(\rho/a)^2 \bar{\varepsilon}(\phi)$ in the expansion of Eq. (7), instead of Eq. (9) we obtain

$$(\hat{\mathbf{H}}_0 + h\hat{\mathbf{U}})F(\rho, \phi) = \beta^2 F(\rho, \phi), \quad (11)$$

where $\hat{\mathbf{U}} = 2k_2^2 \Delta(\rho/a)^2 f(\phi)$, $\bar{\varepsilon}(\phi) = hf(\phi)$, and $h \ll 1$ is an azimuthal-refractive-index perturbation strength parameter. The extra perturbed potential $\hat{\mathbf{U}}$ introduces correction terms in the $\beta_{l,p}^2$. The normalized first-order correction term is written as (for nondegenerate modes)

$$[\bar{\beta}_{l,p}^{(1)}]^2 = \frac{\Delta}{V} \int_0^\infty \text{LG}_l^p(\rho') \rho' \text{LG}_l^p(\rho') d\rho' \int_0^{2\pi} f(\phi) d\phi. \quad (12)$$

A detailed study on corrections is provided in Appendix A [26–47]. The normalized second-order correction term is given as

$$[\bar{\beta}_{l,p}^{(2)}]^2 = \frac{\Delta}{4V} \sum_{(l',p') \notin D(l,p)} \left(\frac{|\int_0^\infty \text{LG}_{l'}^{p'}(\rho') \rho' \text{LG}_l^p(\rho') d\rho' \int_0^{2\pi} e^{-il'\phi} f(\phi) e^{il\phi} d\phi|^2}{|l'| - |l| + 2(p' - p)} \right), \quad (13)$$

where $D(l, p)$ denotes a degenerate subspace of modes that have the same $\beta_{l,p}$. If we define the normalized effective refractive index as $b = (\bar{n} - n_{\text{clad}})/(n_{\text{core}} - n_{\text{clad}})$, then

$$b \approx 1 - \frac{2(|l| + 2p + 1)}{V} + \frac{h}{2\Delta} [\bar{\beta}_{l,p}^{(1)}]^2 + \frac{h^2}{2\Delta} [\bar{\beta}_{l,p}^{(2)}]^2. \quad (14)$$

Note the inclusion of β^2 instead of $\beta_{l,p}^2$ in Eq. (9) and we introduce $\xi = 1 - 2\Delta(\rho/a)^2$ to obtain

$$\sum_{l,p} \left[\text{LG}_l^p \left(\frac{d^2 S_{l,p}}{dz^2} + 2ik_2 \frac{dS_{l,p}}{dz} \right) + k_2^2 [\dots + \bar{\varepsilon}_{-1} \xi(\rho) \text{LG}_{l+m_0}^p S_{l+m_0,p} + (\beta^2 - k_2^2) \text{LG}_l^p S_{l,p} + \bar{\varepsilon}_1 \xi(\rho) \text{LG}_{l-m_0}^p S_{l-m_0,p} + \dots] e^{il\phi} \right] = 0. \quad (15)$$

By using the orthogonality of $\text{LG}_l^p(\rho)e^{il\phi}$ functions, i.e.,

$$\int_0^\infty \int_0^{2\pi} (\text{LG}_{l'}^{p'})^* e^{-il'\phi} \text{LG}_l^p e^{il\phi} \rho d\phi d\rho = \delta_{l,l'} \delta_{p,p'},$$

in Eq. (15) we obtain the equation

$$\frac{d^2 S_{l',p'}}{dz^2} + 2ik_2 \frac{dS_{l',p'}}{dz} + (\beta^2 - k_2^2) S_{l',p'} + 2\pi k_2^2 \sum_{l,p} [\dots + \bar{\epsilon}_{-1} f_{l',l+m_0}^{p',p} S_{l+m_0,p} + \bar{\epsilon}_1 f_{l',l-m_0}^{p',p} S_{l-m_0,p} + \dots] = 0, \quad (16)$$

where

$$f_{l',l}^{p',p} = \int_0^\infty (\text{LG}_{l'}^{p'})^* \xi(\rho) \text{LG}_l^p \rho d\rho$$

are overlap coefficients between the modes (l', p') and (l, p) , through the coupling potential $\xi(\rho)$.

It is clear from Eq. (16) that the coefficients $S_{l',p'}$ for various (l', p') are coupled and the coupling is governed by both the mode overlap coefficients $f_{l',l}^{p',p}$ and the azimuthal Fourier components $\bar{\epsilon}_q$. For N coupled modes which are allowed by the modal dispersion equation of basis modes, given by Eq. (14), we solve for $S_{l',p'}(z)$ by expressing Eq. (16) in a matrix form, given as

$$\begin{bmatrix} S_{l',p'}' \\ S_{l',p'}'' \end{bmatrix}_{2N \times 1} = \mathbf{A} \begin{bmatrix} S_{l',p'} \\ S_{l',p'}' \end{bmatrix}_{2N \times 1},$$

where $S_{l',p'}' = dS_{l',p'}/dz$, $S_{l',p'}'' = d^2 S_{l',p'}/dz^2$, and the matrix \mathbf{A} consists of elements $\bar{\epsilon}_q$ and the overlap coefficients $f_{l',l}^{p',p}$. Thus, the coupled equation (16) can be written as

$$\frac{d\bar{\mathcal{S}}}{dz} = \mathbf{A}\bar{\mathcal{S}}, \quad (17)$$

where $\bar{\mathcal{S}} = \begin{bmatrix} S_{l',p'} \\ S_{l',p'}' \end{bmatrix}_{2N \times 1}$.

We solve Eq. (17) as a matrix eigenvalue problem such that the solution for $S_{l',p'}(z)$ is given as

$$S_{l',p'}(z) = \sum_m C_m S_{l',p',m} e^{ik_0 \lambda_m (z-z_1)}, \quad (18)$$

where $S_{l',p',m}$ is the (l', p') th row of the eigenvector matrix of \mathbf{A} and λ_m are the eigenvalues of \mathbf{A} , which consist of both forward and backward propagating waves. The unknown constants C_m are calculated by applying boundary conditions at positions z_1 and z_2 , the input and output interfaces of the finite-size GRAIN medium, respectively. The field in medium 1 is

$$E_1(\rho, \phi, z) = E_i + \sum_{l,p} R_{l,p} \text{LG}_l^p(\rho) e^{il\phi} e^{-ik_1(z-z_1)}, \quad (19)$$

where an LG beam of mode (l_0, p_0) is incident:

$$E_i(\rho, \phi, z) = \text{LG}_{l_0}^{p_0}(\rho) e^{il_0\phi} e^{ik_1 z}.$$

The field in medium 3 is

$$E_3(\rho, \phi, z) = \sum_{l,p} T_{l,p} \text{LG}_l^p(\rho) e^{il\phi} e^{ik_3(z-z_2)}, \quad (20)$$

where $R_{l,p}$ and $T_{l,p}$ are the $N + N$ normalized complex amplitudes of the reflected and transmitted modes with respect

to the incident beam amplitude, respectively. Imposing the boundary conditions, i.e., E along \hat{x} and H along \hat{y} being continuous at $z = z_1$ and $z = z_2$, where

$$H_y = \frac{-i}{\omega\mu_0} \frac{\partial E_x}{\partial z},$$

the following equations are obtained:

$$e^{ik_1 z_1} \delta_{l,l_0} \delta_{p,p_0} + R_{l,p} = S_{l,p}(z_1), \quad (21)$$

$$ik_1 e^{ik_1 z_1} \delta_{l,l_0} \delta_{p,p_0} - ik_1 R_{l,p} = ik_2 S_{l,p}(z_1) + \left. \frac{dS_{l,p}}{dz} \right|_{z=z_1}, \quad (22)$$

$$T_{l,p} = S_{l,p}(z_2) e^{ik_2(z_2-z_1)}, \quad (23)$$

$$ik_3 T_{l,p} = \left(ik_2 S_{l,p}(z_2) + \left. \frac{dS_{l,p}}{dz} \right|_{z=z_2} \right) e^{ik_2(z_2-z_1)}. \quad (24)$$

Equations (21)–(24) provide $4N$ constraint equations with $R_{l,p}$, $T_{l,p}$, and C_m as the $N + N + 2N$ unknowns, and these are solved algebraically as a system of linear equations. The total reflected intensity R and total transmitted intensity T are defined as

$$R = \sum_{l,p} |R_{l,p}|^2, \quad T = \sum_{l,p} |T_{l,p}|^2$$

and the total intensity $R + T = 1$, for a nonabsorbing GRAIN medium.

III. RESULTS AND DISCUSSION

The azimuthal variation of the refractive index provides orbital angular momentum to the input light field. However, due to the intimate relation between the radial-index and azimuthal-index modes, the azimuthal coupling along the propagation direction also leads to the coupling of the radial-index modes of the LG beam. This is a distinct feature arising due to the propagation dynamics in such devices. We use the detailed analysis presented earlier, which models the light propagation through the GRAIN fiber element, for further control of LG basis modes. We have undertaken all calculations using MATLAB. The algorithm is the following. First, we compute the Fourier content of the azimuthal-refractive-index dependence using Eq. (3). These Fourier components and other overlapping coefficients in Eq. (16) are computed numerically and are expressed in matrix A . Matrix A is solved for eigenvalues and eigenvectors, which determine the LG mode strength within the medium equation (18). Further, using the boundary conditions given in Eqs. (23) and (24), we obtain the transmission coefficients for each LG mode as these

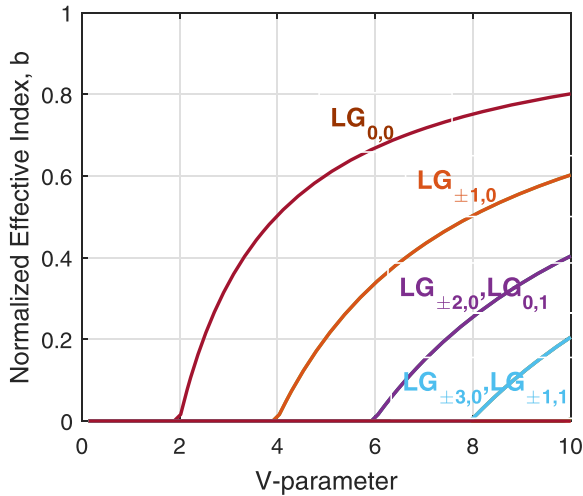


FIG. 2. Dependence of the normalized effective refractive index of the LG basis modes on the V parameter. We are working with the V parameter such that a few lower-order modes are controlled within the GRAIN fiber element.

vary along the finite propagation length of the fiber and are shown in Figs. 3, and 4, 6. Their wavelength dependence is shown in Figs. 5 and 7. Additionally, coherent superposition state generation in the GRAIN fiber is demonstrated. Here the specific nature of the superposition state is validated using the following protocol. As the specific superposed state is provided as input, it results in a complete periodic revival of the initial input superposition state. Thus, a specific superposition state generation is mapped to the specific input superposition state; further details are provided in Appendix B.

Here the underlying GRIN structure leads to cutoff criteria, and the finite set of basis modes are identified, in accordance with the dispersion relation provided in Eq. (14), which is plotted in Fig. 2. We observe that the impact of the azimuthal coupling on the normalized effective refractive index is negligible when $h = \Delta/11$. Therefore, we present these calculations at this h value. However, we have discussed larger azimuthal couplings and the resulting changes in the dispersion relation in Appendix A. We present some generic results for two cases of the V parameter, i.e., $V = 5$ and 7, such that three modes ($LG_{0,0}$, $LG_{1,0}$, and $LG_{-1,0}$) and six modes ($LG_{0,0}$, $LG_{1,0}$, $LG_{-1,0}$, $LG_{0,1}$, $LG_{2,0}$, and $LG_{-2,0}$) are allowed, respectively. Our mathematical treatment can accommodate any azimuthal-refractive-index dependence. However, we consider the cosinusoidal azimuthal-refractive-index function $\bar{\epsilon}(\phi) = h \cos(m_0\phi)$ for all the switching results, which is insensitive to OAM handedness. Further, we provide calculations of a linearly varying azimuthal refractive index $\bar{\epsilon}(\phi) = h\phi$ for accessing the handedness of the OAM modes.

A. Cosinusoidal variation in the GRAIN fiber element

The allowed OAM modes that propagate in the first case of the parameter $V = 5$ are shown in Fig. 3. We solve numerically for $m_0 = 1$ and $\Delta = 0.01$ with the incident Gaussian mode $(l, p) = (0, 0)$. Because of the periodicity of the azimuthal refractive index, the OAM modes couple to each other and generate equal magnitude OAM ($l = \pm 1, p = 0$) modes

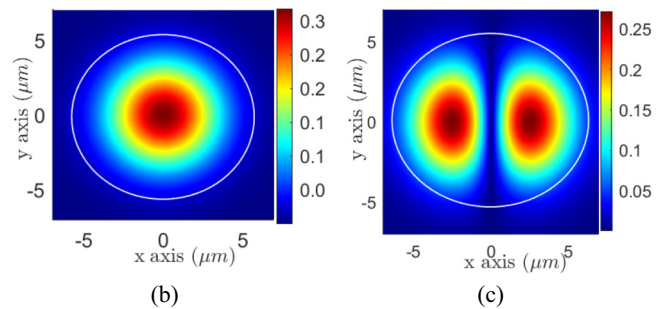
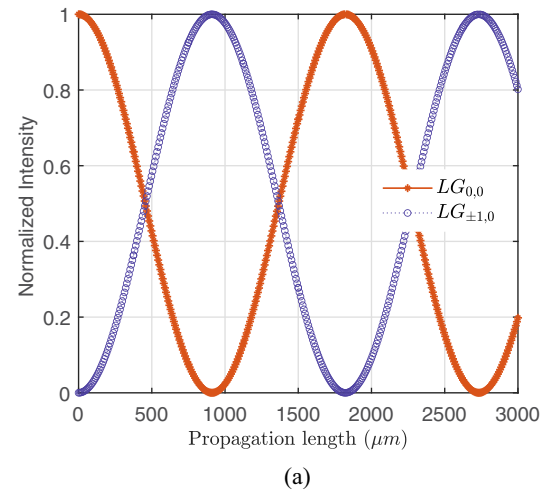


FIG. 3. (a) Input Gaussian mode: $(l, p) = (0, 0)$ switches to $(l = \pm 1, p = 0)$ at a propagation length of $900 \mu\text{m}$ and $\lambda = 1.5 \mu\text{m}$. The energy exchange happens periodically between the modes. The transverse intensity profiles of the modes (b) $l = 0$ and (c) $l = \pm 1$ are shown below, with a core radius $a = 5.627 \mu\text{m}$ (shown as a white circle) and a beam waist $\rho_0 = 2.516 \mu\text{m}$.

(due to the rotational invariance of clockwise and counterclockwise OAM modes). We plot in Fig. 3(a) the sum of each OAM mode intensity ($I = I_l + I_{-l}$), and the mode is shown in Fig. 3(c). Similarly, we have computed the mode evolution for the parameters $V = 7$ and $m_0 = 2$. The corresponding results are plotted in Fig. 4, where periodic switching is observed and a complete conversion to the radial-index mode ($l = 0, p = 1$) of the LG beam is seen.

Thus, the periodic exchange of energy between the OAM content and the radial-index modes of the LG beam for $m_0 = 1$ and $m_0 = 2$, respectively, can be used to address the issue of crosstalk in the context of WDM with LG modes. A typical WDM protocol involves a series of channels centered at different wavelengths with a specific bandwidth. The isolation of adjacent channels depends on the frequency bandwidth of the channels as well as the field mode overlap between the adjacent channels. We show in Fig. 5 that one can lift the fundamental mode of every alternate even channel to the higher-order mode $LG_{\pm 1,0}$, whereas the odd channels continue to remain in the fundamental mode $LG_{0,0}$ for $m_0 = 1$. Similarly, we switch the Gaussian mode $LG_{0,0}$ to the radial-index mode $LG_{0,1}$ of the LG beam for $m_0 = 2$. Hence, such an implementation will lead to the spatial modes of the adjacent channels having significant refractive-index contrast in a typical multimode fiber with a V number of approximately 5 and

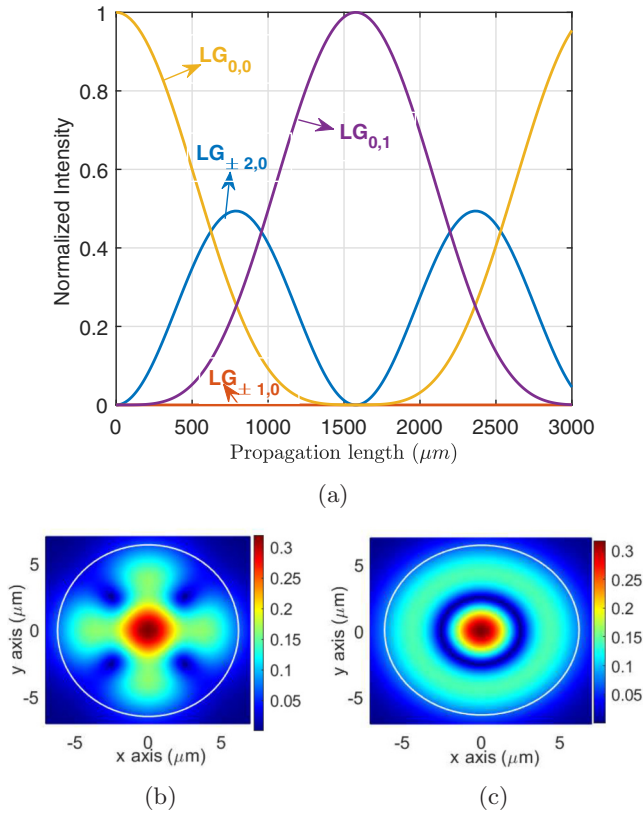


FIG. 4. (a) Input Gaussian mode: $(l, p) = (0, 0)$ switches to the radial-index mode $(l = 0, p = 1)$ of the LG beam at a propagation length of $1600 \mu\text{m}$ and $\lambda = 1.5 \mu\text{m}$ for $V = 7$ and $m_0 = 2$. Also shown are the transverse intensity profiles: (b) an equal magnitude superposition state of four modes ($LG_{2,0}$, $LG_{-2,0}$, $LG_{0,0}$, and $LG_{0,1}$) at the propagation length of $750 \mu\text{m}$ and (c) radial-index mode $LG_{0,1}$ with a core radius $a = 7.878 \mu\text{m}$ (shown as a white circle) and a beam waist $\rho_0 = 2.977 \mu\text{m}$.

7 [14]. This would drastically minimize the crosstalk between adjacent channels and effectively double the bandwidth for the even (odd) channels in the higher-order (fundamental) mode scenario within the fiber. The result is depicted in Fig. 5, which uses the GRAIN fiber of propagation length 50 mm, allowing access to ten OAM mode switching channels and six radial-index mode (p index of the LG beam) switching wavelength channels for $m_0 = 1$ and 2, respectively, in the 1.3 – $1.55 \mu\text{m}$ wavelength range of optical communication. The number of channels that can be accessed depends on the propagation length of the GRAIN fiber element and the strength of the azimuthal coupling.

We observe the access of 20 WDM channels for OAM mode switching and 12 WDM channels for radial-index mode (p index of the LG beam) switching for a propagation length of 100 mm and $h = \Delta/11 = 0.0009$, in addition to the result of accessing 51 WDM channels for OAM mode switching and 30 WDM channels for radial-index mode (p index of the LG beam) switching for the propagation length of 50 mm and $h = \Delta/2 = 0.005$. It should be noted that more WDM channels are accessed for spatial mode switching as the propagation length of the fiber element or modulation strength

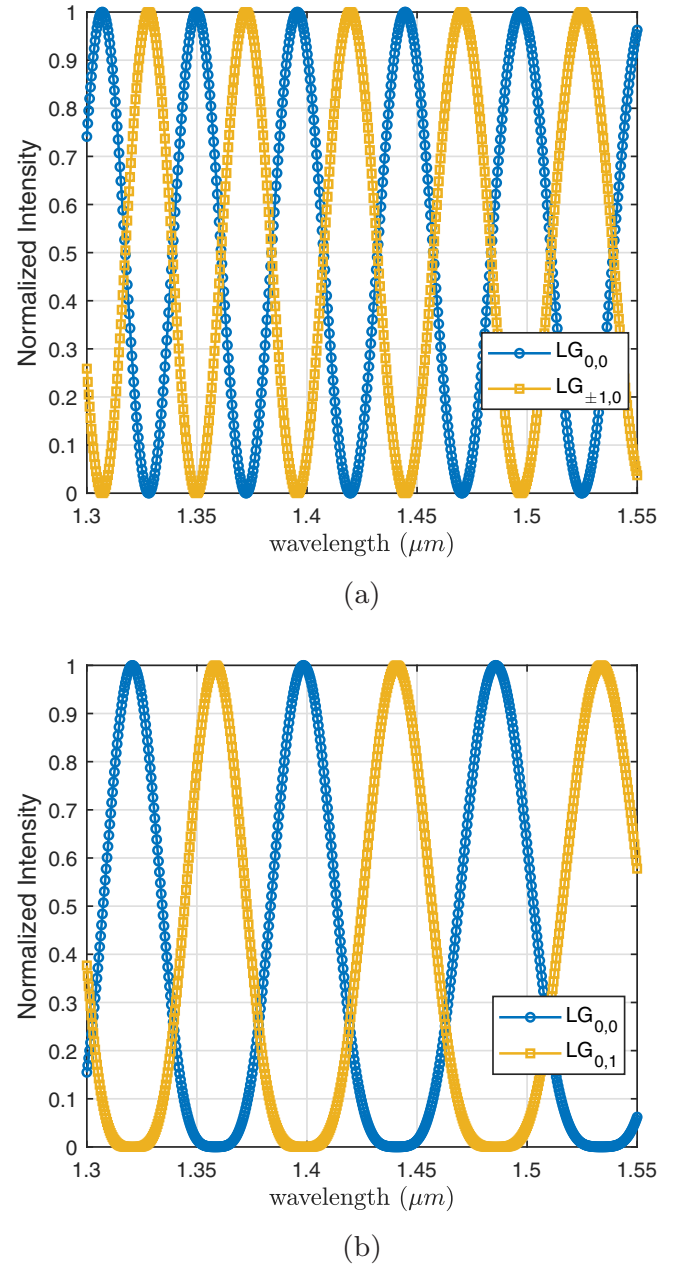


FIG. 5. Total of ten WDM channels of OAM mode switching and six WDM channels of radial-index mode switching accessible for the GRAIN fiber of propagation length 50 mm for (a) $m_0 = 1$ and $V = 5$ and (b) $m_0 = 2$ and $V = 7$. The adjacent wavelength channels are converted from (a) $(l = 0, p = 0)$ to $(l = \pm 1, p = 0)$ and (b) $(l = 0, p = 0)$ to $(l = 0, p = 1)$, which helps in reducing the crosstalk between adjacent wavelength channels.

increases; however, a decrease in the switching efficiency of the radial-index mode of the LG beam is observed.

Hence, the periodic energy exchange along the propagation length of the GRAIN fiber element between the $LG_{0,0}$ and $LG_{\pm 1,0}$ modes for $m_0 = 1$ and also between the $LG_{0,0}$ and $LG_{0,1}$ modes for $m_0 = 2$ is exploited to arrange adjacent WDM channels to acquire additional OAM or the radial-index mode of the LG beam. Therefore, such an optical element

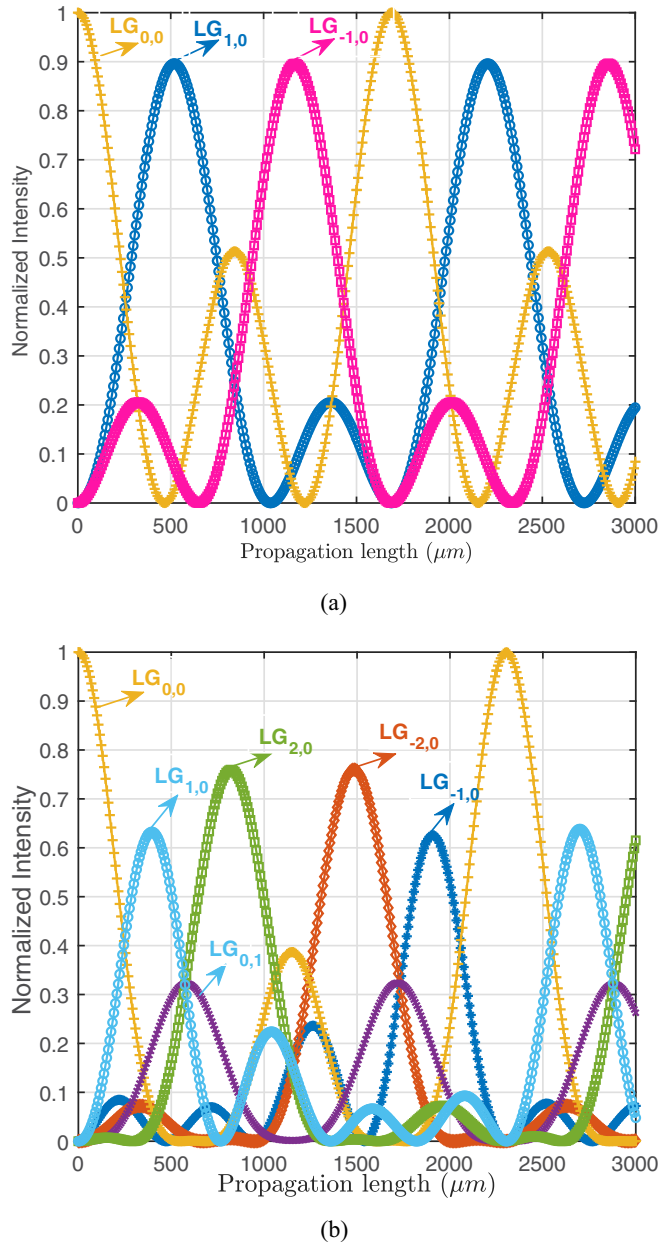


FIG. 6. Linearly varying GRAIN fiber element: (a) input Gaussian mode $(l, p) = (0, 0)$ switches to $(l = 1, p = 0)$ and $(l = -1, p = 0)$ at propagation lengths of 500 and 1200 μm , respectively, at $\lambda = 1.5 \mu\text{m}$ for $V = 5$ (corresponds to a core radius of 5.627 μm and a beam waist $\rho_0 = 2.516 \mu\text{m}$), and (b) input Gaussian mode $(l, p) = (0, 0)$ switches to $(l = 1, p = 0)$ and $(l = 2, p = 0)$, $(l = -2, p = 0)$, and $(l = -1, p = 0)$ at the propagation lengths of 400, 800, 1500, and 1900 μm , respectively, at $\lambda = 1.5 \mu\text{m}$ for $V = 7$ (corresponds to a core radius of 7.878 μm and a beam waist $\rho_0 = 2.977 \mu\text{m}$)

could be integrated within multimode fiber-based WDM optical communication applications for improved performance.

For a cosinusoidal GRAIN fiber of $m_0 = 1$ and $V = 7$, we have six modes such as $\text{LG}_{2,0}$, $\text{LG}_{1,0}$, $\text{LG}_{0,0}$, $\text{LG}_{0,1}$, $\text{LG}_{-1,0}$, and $\text{LG}_{-2,0}$. At around 1300 μm , $(\text{LG}_{2,0} - \text{LG}_{0,1} + \text{LG}_{-2,0})/\sqrt{3}$, an equal magnitude superposition state, is generated. In a typical multimode or GRIN fiber, the modes in

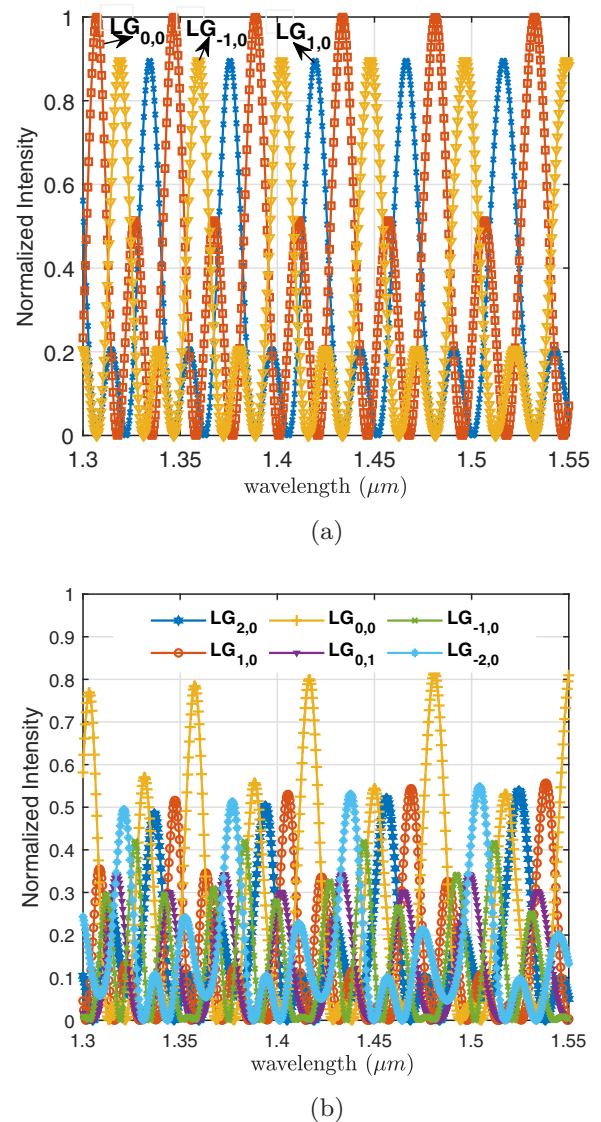


FIG. 7. Wavelength switching in the linear GRAIN fiber. (a) Each handedness of the OAM mode is accessed at different wavelengths with an efficiency of about 90% for $V = 5$. (b) Inclusion of the higher spatial modes with the efficiency of access about 50% for $V = 7$.

the above superposition state degenerate and propagate with the same β . One can thus switch from the $\text{LG}_{0,0}$ Gaussian mode to the superposition state and vice versa, as shown in Appendix B. Using $m_0 = 1$ and $V = 9$, a few radial-index modes such as $\text{LG}_{\pm 1,1}$ with efficiency about 65% and $\text{LG}_{0,1}$ with about 80% can be accessed at propagation lengths around 2800 and 3800 μm , respectively. Furthermore, it is observed that the generated OAM modes are integer multiples of the periodicity of GRAIN fiber. Once the particular OAM mode (l index) with $p = 0$ is generated, it couples to the radial-index modes ($p > 0$) of the associated l index. Otherwise, the corresponding radial-index modes of the LG beam are also not generated. Therefore, the azimuthal-refractive-index periodicity dictates the generation of OAM with $p = 0$ and the corresponding radial-index modes of the LG beam.

B. Linear variation in the GRAIN fiber element

We observe that the cosinusoidal azimuthal refractive index always results in an equal magnitude of the $\pm l$ OAM modes. It restricts the possibility of accessing a particular handed OAM mode. In this regard, a linearly varying GRAIN fiber element provides a solution. The field evolution is computed for the V parameter $V = 5$ and 7 . We notice that $V = 5$ leads to the coupling of just three modes, which allows the accessing of $LG_{1,0}$ and $LG_{-1,0}$ at two different propagation lengths with an efficiency of nearly 90%, as shown in Fig. 6(a). The same is manifested in the wavelength switching of the two OAM modes with different handedness, in addition to the $LG_{0,0}$ Gaussian mode; as a result, we can access these three different spatial modes in the WDM protocol, as shown in Fig. 7(a). Similarly, we identify that in Fig. 6(b), five spatial modes can be accessed in the WDM protocol. However, the efficiency of $LG_{1,0}$ and $LG_{-1,0}$ is around 60% and that of $LG_{2,0}$ and $LG_{-2,0}$ is around 70%, which is certainly better in comparison to other implementations of multimode excitation of OAM modes in a fiber [1].

In Fig. 7(a) we show that 17 spatial mode channels can be accessed, with each spatial mode occurring alternately with two-wavelength-channel separation in the wavelength range of 1.3–1.55 μm . These channels can propagate in a vortex fiber, which supports the individual handedness of the OAM modes and exhibits less modal crosstalk. Similarly, Fig. 7(b) illustrates the access of five OAM mode wavelength channels for $V = 7$, but the conversion efficiency is only about 50%.

We anticipate that the proposed GRAIN fiber element can be fused with conventional fiber channels and excites these modes, which include the handedness of the OAM modes and the radial-index mode of the LG beam, as well as their superpositions with wavelength selectivity. This would result in a significant enhancement in multimode optical fiber communications. Furthermore, the recent review of Yang *et al.* [48] emphasizes that both the theory and experiments of fiber-based spatial mode generation are still at an early stage and therefore offer very little control and switching capability. Therefore, our proposed wavelength-tunable GRAIN fiber element could play a significant role in applications such as fiber-based laser sources and sensors and improve WDM-based protocols.

IV. CONCLUSION

We have systematically captured in a theoretical analysis a rather general treatment that can be adapted to any arbitrary azimuthal variation of the refractive index and the resulting effects on the OAM and radial-index mode of the LG beam. In particular, the proposed GRAIN fiber element can be used to substantially minimize the crosstalk in the adjacent WDM channels in multimode fiber-optic communications. We have presented a simulation involving ten channels of alternate OAM mode switching and six channels of alternate radial-index mode switching in the optical communication wavelength range of 1.3–1.55 μm . We envisage immense potential for effective manipulation of the higher-order spatial mode content in the proposed GRAIN element as a powerful fiber-based OAM manipulating element in various

TABLE I. Perturbative correction term values for $\bar{\varepsilon}(\phi) = h\phi$.

Mode	$[\bar{\beta}_{l,p}^{(1)}]^2$ in $(\Delta/2V)$	$[\bar{\beta}_{l,p}^{(2)}]^2$ in $(\Delta/16V)$
$LG_{0,0}$	12.5244	150.45
$LG_{1,0}$	25.1326	323.3946
$LG_{2,0}$	37.6992	485.9426

applications across multiple areas. The GRAIN fiber can be an important tool for manipulating single-photon superposition states. With advantages such as efficient superposition state generation, a small spatial footprint, and ready integrability with conventional fiber optic communication channels, the GRAIN fiber element can become a versatile tool for OAM manipulation.

APPENDIX A: NONDEGENERATE PERTURBATIVE CORRECTIONS OF β^2

Linear GRAIN fiber

In GRIN fiber, nondegenerate modes are identified by the parameter $g = |l| + 2p + 1$, which has the same propagation constant β . We provide the first- and second-order corrections to β^2 in terms of Δ/V in Table I.

The overall β^2 is given as

$$\beta^2 \approx k_2^2 \left(1 - \frac{4g\Delta}{V} + h[\beta_{l,p}^{(1)}]^2 + h^2[\beta_{l,p}^{(2)}]^2 \right). \quad (\text{A1})$$

For example, $g = 1$ for $LG_{0,0}$, the β^2 is given as $\beta^2 = k_2^2 [1 - \frac{1}{V}(4\Delta - \frac{12.5244}{2}h\Delta - \frac{150.45}{16}h^2\Delta)]$. For the cosinusoidal GRAIN fiber, the first-order correction is negligible, arising from the symmetry arguments. Thus, the dispersion curves and cutoff criteria exhibit little change even for large h , quite unlike the linear case (see Fig. 8).

APPENDIX B: SUPERPOSITION STATE AS INPUT TO THE GRAIN FIBER

We have studied the GRAIN fiber with a superposition state as an input. The specific superposition state $(LG_{2,0} - LG_{0,1} + LG_{-2,0})/\sqrt{3}$ is employed as input. We have observed that the input superposition state generates the Gaussian mode. If the right composition of the superposition state is not considered, it does not produce the Gaussian mode with 100% efficiency. For example, the state $(LG_{2,0} - LG_{0,1} + LG_{-2,0})/\sqrt{3}$ in Fig. 9 produces the complete Gaussian mode, whereas flipping the sign of the radial-index mode of the LG beam phase with respect to the other, i.e., $(LG_{2,0} + LG_{0,1} + LG_{-2,0})/\sqrt{3}$, can only generate the Gaussian mode with 10% efficiency. Since the correct superposition state is only mapped to the input state, it signifies the coherent evolution of each mode in the composition, which indicates that the superposition states that are generated by the GRAIN are not incoherent intensity mixtures; they are the coherent amplitude superposition states. This can be used to switch the superposition state into a Gaussian mode at each wavelength channel of WDM.

It is demonstrated that the GRAIN fiber element can generate the superposition of a specific set of radial-azimuthal

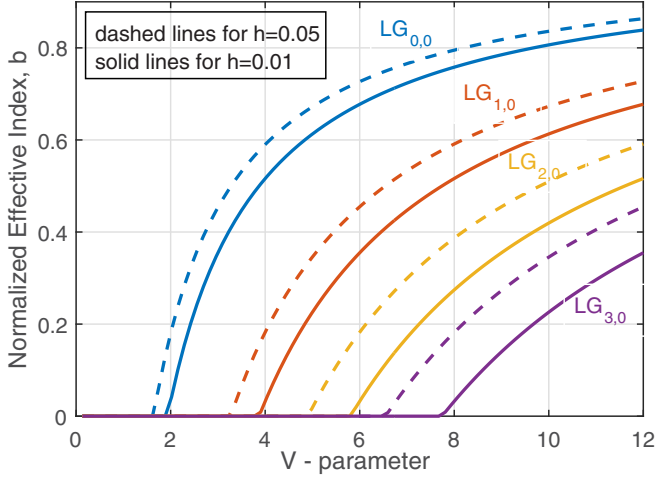


FIG. 8. Dispersion curves of the linear GRAIN fiber. The above curves are for nondegenerate modes only. One can anticipate splitting the curves among the degenerate modes due to the azimuthal coupling. Solid dispersion curves indicate a slight change in the cutoff criteria of spatial modes compared with the unperturbed case. The number of spatial modes supported for a given V parameter remains the same as the $h = \Delta = 0.01$ case. When $h = 5\Delta = 0.05$ (dashed dispersion curves), the number of spatial modes supported by the GRAIN fiber changes for a given V parameter.

modes of the LG beam. However, a few sets of spatial modes are permitted by choosing the radial boundary condition of the optical fiber, which sets the V parameter, allowing precise control of the creation of superposition states. The generation of superposition states is also necessary for high-dimensional state transfer and manipulation, quantum teleportation, quantum cryptography, and all-optical computation [49–52].

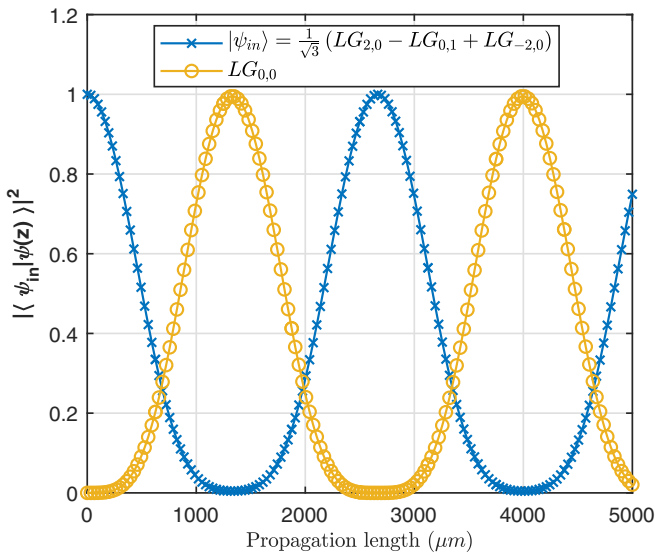


FIG. 9. Superposition state propagation in the GRAIN fiber, showing periodic revival of the input state $(LG_{2,0} - LG_{0,1} + LG_{-2,0})/\sqrt{3}$ between the Gaussian modes.

APPENDIX C: SPIN-ORBIT-INTERACTION IN THE GRAIN FIBER

The full wave equation is given as

$$\nabla^2 \mathbf{E} + k_0^2 \epsilon_r(\rho, \phi) \mathbf{E} = \vec{\nabla}(\vec{\nabla} \cdot \mathbf{E}). \quad (\text{C1})$$

The divergence term on the right-hand side contributes to the spin-orbit interaction. This can be expressed for a nonconducting medium as

$$\vec{\nabla} \cdot \mathbf{D} = 0. \quad (\text{C2})$$

By using $\mathbf{D} = \epsilon_r(\rho, \phi) \mathbf{E}$ in (C2), it can be rewritten as

$$\vec{\nabla} \cdot \mathbf{E} = -\mathbf{E} \cdot \vec{\nabla} \ln[\epsilon_r(\rho, \phi)]. \quad (\text{C3})$$

In this equation, one can see the interaction of polarization, called the spin angular momentum (SAM) of light, with the refractive-index gradient. This is the starting point for spin-orbit interactions. To further clarify, consider that the electric field has transverse components, that is, $\mathbf{E} = (E_\rho, E_\phi)$ and $\epsilon_r(\rho, \phi) = \epsilon_\rho(\rho)\epsilon_\phi(\phi)$, and Eq. (C3) results in

$$-\vec{\nabla} \cdot \mathbf{E} = \frac{E_\rho}{\epsilon_\rho} \frac{\partial \epsilon_\rho}{\partial \rho} + \frac{E_\phi}{\rho \epsilon_\phi} \frac{\partial \epsilon_\phi}{\partial \phi}. \quad (\text{C4})$$

The difference in this equation in comparison to the specialty fibers arises from the consideration of only one term of the radial derivative. In our case, as a result of the radial GRIN function, we also expect the spin-orbit interaction (SOI) to exist in the GRAIN fiber. The SOI is observed due to the graded radial refractive index of the fiber. To get to the SOI term, which is listed in [53,54], we write $\vec{\nabla}(\vec{\nabla} \cdot \mathbf{E})$ as

$$\begin{aligned} \vec{\nabla}(\vec{\nabla} \cdot \mathbf{E}) = & \left(\frac{\partial \ln(\epsilon_\rho)}{\rho \partial \rho} \hat{\mathbf{L}} \hat{\mathbf{S}} + \frac{\partial \ln(\epsilon_\rho)}{\partial \rho} \frac{\partial}{\partial \rho} + \frac{\partial^2 \ln(\epsilon_\rho)}{\partial \rho^2} \right) E_\rho \hat{\rho} \\ & + \left[\left(\frac{\partial \ln(\epsilon_\phi)}{\rho \partial \phi} \frac{\partial}{\partial \rho} - \frac{\partial \ln(\epsilon_\phi)}{\rho^2 \partial \phi} \right) \hat{\mathbf{S}} \right. \\ & \left. + \frac{\partial \ln(\epsilon_\phi)}{\rho^2 \partial \phi} \hat{\mathbf{L}} + \frac{\partial^2 \ln(\epsilon_\phi)}{\rho^2 \partial \phi^2} \right] E_\phi \hat{\phi}. \end{aligned} \quad (\text{C5})$$

We identify the OAM operator as $\hat{\mathbf{L}} = -i \frac{\partial}{\partial \phi}$ and the SAM operator as

$$\hat{\mathbf{S}} \hat{\rho} = i \hat{\phi}, \quad \hat{\mathbf{S}} \hat{\phi} = -i \hat{\rho}. \quad (\text{C6})$$

We can see that the first three terms on the right-hand side of Eq. (C5) contain the usual terms, but due to azimuthal coupling, other possibilities arise. The spin-orbit-interaction term is given as

$$\hat{\mathbf{H}}_{SO} = \frac{\partial \ln(\epsilon_\rho)}{\rho \partial \rho} \hat{\mathbf{L}} \hat{\mathbf{S}}. \quad (\text{C7})$$

Furthermore, the change in the phase of the propagation constant is given by

$$\delta(\beta^2) = \langle \Psi | \hat{\mathbf{H}}_{SO} | \Psi \rangle = \int \Psi^* \frac{\partial \ln(\epsilon_\rho)}{\rho \partial \rho} \hat{\mathbf{L}} \hat{\mathbf{S}} \Psi \rho d\rho d\phi. \quad (\text{C8})$$

By approximating $\delta(\beta^2) \approx 2\beta \delta\beta$ and considering $\epsilon_\rho = \epsilon_2 [1 - 2\Delta(\rho/a)^2]$ and $\Psi = LG_l^p(\rho) e^{il\phi} e^{i\beta z} |s\rangle$, the operators

lead to $\hat{L}\Psi = l\Psi$, where l is the OAM, and $\hat{S}\Psi = s\Psi$, where s is the SAM, which takes the value 1 or -1 for right circular or left circular polarizations, respectively. Equation (C8) becomes

$$\delta\beta = \frac{-\lambda\Delta l s}{\pi a^2}. \quad (\text{C9})$$

One can now compute that the superposition of the OAM mode and the SAM mode results in different phase evolution along the propagation length. It results in two types of SOI: parallel SOI when the OAM and SAM signs are aligned and antiparallel SOI when the signs are not aligned. To compare

the strength of SOI in our GRAIN fiber, we use a Δ of 0.05, a wavelength of $0.8 \mu\text{m}$, and a core radius of $3 \mu\text{m}$ for $V = 7$ to support an OAM equal to 2. Then $\delta\beta = 28.3 \text{ cm}^{-1}$, which is of the same order of magnitude (i.e., 22.1 cm^{-1}) as mentioned in [53] for the dispersion-tailored few-mode fiber. The SOI term is contributed only by the radial refractive index (GRIN fiber) medium; however, the azimuthal refractive index does not contribute to the SOI. The strict condition, however, is that Δ/a^2 be as small as possible (i.e., $\delta\beta \ll \beta$). The GRAIN fiber offers other possibilities, such as spin-radial coupling, which is beyond the scope of the present paper.

-
- [1] Y. Shen, X. Wang, Z. Xie, C. Min, X. Fu, Q. Liu, M. Gong, and X. Yuan, *Light Sci. Appl.* **8**, 90 (2019).
- [2] A. Forbes, A. Dudley, and M. McLaren, *Adv. Opt. Photon.* **8**, 200 (2016).
- [3] J. Wang and Y. Liang, *Front. Phys.* **9**, 688284 (2021).
- [4] D. L. Andrews and M. Babiker, *The Angular Momentum of Light* (Cambridge University Press, Cambridge, 2013).
- [5] R. Chen, H. Zhou, M. Moretti, X. Wang, and J. Li, *IEEE Commun. Surv. Tutor.* **22**, 840 (2020).
- [6] M. Ma, Y. Lian, Y. Wang, and Z. Lu, *Front. Phys.* **9**, 773505 (2021).
- [7] L. Feng, Y. Li, S. Wu, W. Li, J. Qui, H. Guo, X. Hong, Y. Zuo, and J. Wu, *Appl. Sci.* **9**, 2408 (2019).
- [8] C. Caucheteur, J. Villatoro, F. Liu, M. Loyez, T. Guo, and J. Albert, *Adv. Opt. Photon.* **14**, 1 (2022).
- [9] Y. Han, Y.-G. Liu, Z. Wang, W. Huang, L. Chen, H.-W. Zhang, and K. Yang, *Nanophotonics* **7**, 287 (2018).
- [10] H. Zhang, B. Mao, Y. Han, Z. Wang, Y. Yue, and Y. Liu, *Appl. Sci.* **9**, 1033 (2019).
- [11] H. Huang *et al.*, *Sci. Rep.* **5**, 14931 (2015).
- [12] C. He *et al.*, *Nat. Commun.* **10**, 4264 (2019).
- [13] P. Gregg, P. Kristensen, and S. Ramachandran, *Opt. Express* **24**, 18938 (2016).
- [14] G. P. Agarwal, *Nonlinear Fiber Optics* (Academic, New York, 2019), Chap. 14.
- [15] S. Li and J. Wang, *Opt. Express* **23**, 18736 (2015).
- [16] X. M. Xi, G. K. L. Wong, M. H. Frosz, F. Babic, G. Ahmed, X. Jiang, T. G. Euser, and P. S. J. Russell, *Optica* **1**, 165 (2014).
- [17] M. Hisatomi, M. C. Parker, and S. D. Walker, *Proceedings of the Optical Fiber Communication Conference and Exposition and the National Fiber Optic Engineers Conference, Anaheim, 2005* (Optica, Washington, DC, 2005), paper OME7.
- [18] M. C. Parker, M. Hisatomi, and S. D. Walker, U.S. Patent No. US 2008/0101754 A1 (1 May 2008).
- [19] W. N. Plick, R. Lapkiewicz, S. Ramelow, and A. Zeilinger, [arXiv:1306.6517](https://arxiv.org/abs/1306.6517).
- [20] M. D. Feit and J. A. Fleck, Jr., *Appl. Opt.* **17**, 3990 (1978).
- [21] S. Chen and J. Wang, *Sci. Rep.* **7**, 3990 (2017).
- [22] J. Albert, L.-Y. Shao, and C. Caucheteur, *Laser Photon. Rev.* **7**, 83 (2013).
- [23] M. G. Moharam and T. K. Gaylord, *J. Opt. Soc. Am.* **71**, 811 (1981).
- [24] E. Nazemosadat, M. Mazur, S. Kruk, I. Kravchenko, J. Carpenter, J. Schröder, P. A. Andrekson, M. Karlsson, and Y. Kivshar, *Adv. Opt. Mater.* **7**, 1801679 (2019).
- [25] A. Forbes, *Laser Photon. Rev.* **13**, 1970043 (2020).
- [26] J. J. Sakurai and J. J. Napolitano, *Modern Quantum Mechanics*, 2nd ed. (Pearson, New York, 2011), Chap. 5.
- [27] L. E. Myers, R. C. Eckardt, M. M. Fejer, R. L. Byer, W. R. Bosenberg, and J. W. Pierce, *J. Opt. Soc. Am. B* **12**, 2102 (1995).
- [28] A. Yariv and P. Yeh, *Optical Waves in Crystals* (Wiley, New York, 2003).
- [29] L. Allen, M. W. Beijersbergen, R. J. C. Spreeuw, and J. P. Woerdman, *Phys. Rev. A* **45**, 8185 (1992).
- [30] F. Gori, *Opt. Lett.* **24**, 584 (1999).
- [31] S. Li and J. Wang, *Sci. Rep.* **5**, 15406 (2015).
- [32] J. Arlt, K. Dholakia, L. Allen, and M. J. Padgett, *J. Mod. Opt.* **45**, 1231 (1998).
- [33] Y. Ma, L. Fang, and G. Wu, *Opt. Commun.* **386**, 1 (2017).
- [34] L. Yang, L. Xue, J. Su, and J. Qian, *Chin. Opt. Lett.* **9**, 070603 (2011).
- [35] G. Volpe and D. Petrov, *Opt. Commun.* **237**, 89 (2004).
- [36] T. Erdogan, *J. Opt. Soc. Am. A* **14**, 1760 (1997).
- [37] J. Zhou, J. Zong, and D. Liu, *Opt. Express* **23**, 31964 (2015).
- [38] N. Zhang, J. Zhu, X. Cai, and S. Yu, *Asia Communications and Photonics Conference, Shanghai, 2014* (OSA, Washington, DC, 2014).
- [39] A. Trichili, C. Rosales-Guzmán, A. Dudley, B. Ndagano, A. B. Salem, M. Zghal, and A. Forbes, *Sci. Rep.* **6**, 27674 (2016).
- [40] M. G. Moharam, E. B. Grann, D. A. Pommert, and T. K. Gaylord, *J. Opt. Soc. Am. A* **12**, 1068 (1995).
- [41] N. Chateau and J. P. Hugonin, *J. Opt. Soc. Am. A* **11**, 1321 (1994).
- [42] P. Yeh, *J. Opt. Soc. Am.* **69**, 742 (1979).
- [43] D. G. Hall, *Opt. Lett.* **21**, 9 (1996).
- [44] R. Simon, E. C. G. Sudarshan, and N. Mukunda, *J. Opt. Soc. Am. A* **3**, 536 (1986).
- [45] Q. Zhan, *Adv. Opt. Photon.* **1**, 1 (2009).
- [46] M. Lax, W. H. Louisell, and W. B. McKnight, *Phys. Rev. A* **11**, 1365 (1975).
- [47] S. M. Barnett, M. Babiker, and M. J. Padgett, *Philos. Trans. R. Soc. A* **375**, 20150444 (2017).
- [48] Y. Yang, Y. Li, and C. Wang, *J. Opt.* **51**, 910 (2022).
- [49] H. Rubinsztein-Dunlop *et al.*, *J. Opt.* **19**, 013001 (2017).

- [50] M. Erhard, R. Fickler, M. Krenn, and A. Zeilinger, *Light Sci. Appl.* **7**, 17146 (2018).
- [51] X. M. Xi, T. Weiss, G. K. L. Wong, F. Biancalana, S. M. Barnett, M. J. Padgett, and S. J. P. Russell, *Phys. Rev. Lett.* **110**, 143903 (2013).
- [52] K. Saitoh and S. Matsuo, *J. Light. Technol.* **34**, 55 (2016).
- [53] D. L. P. Vitullo, C. C. Leary, P. Gregg, R. A. Smith, D. V. Reddy, S. Ramachandran, and M. G. Raymer, *Phys. Rev. Lett.* **118**, 083601 (2017).
- [54] P. Gregg, P. Kristensen, A. Rubano, S. Golowich, L. Marrucci, and S. Ramachandran, *Nat. Commun.* **10**, 4707 (2019).